2024 IEEE/RSJ International Conference on Intelligent Robots and Systems (IROS)
October 14-18, 2024. Abu Dhabi, UAE

Enhancing Surgical Precision in Autonomous Robotic Incisions via Physics-Based Tissue Cutting Simulation

Jiawei Ge[1†*], Ethan Kilmer[2†], Leila J. Mady[3], Justin D. Opfermann[1], and Axel Krieger[1], *Senior Member, IEEE*

***Abstract*— In soft tissue surgeries, such as tumor resections, achieving precision is of utmost importance. Surgeons conventionally achieve this precision through intraoperative adjustments to the cutting plan, responding to deformations from tool-tissue interactions. This study examines the integration of physics-based tissue cutting simulations into autonomous robotic surgery to preoperatively predict and compensate for such deformations, aiming to improve surgical precision and reduce the necessity for dynamic adjustments during autonomous surgeries. This study adapts a real-to-sim-to-real workflow. Initially, the Autonomous System for Tumor Resection (ASTR) was employed to evaluate its accuracy in performing preoperatively intended incisions along the irregular contours of porcine tongue pseudotumors. Following this, a finite element analysis-based simulation, utilizing the Simulation Open Framework Architecture (SOFA), was developed and tuned to accurately mimic these tissue and incision interactions. Insights gained from this simulation were applied to refine the robot's path planning, ensuring a closer alignment of actual incisions with the initially intended surgical plan. The efficacy of this approach was validated by comparing surface incision precision on *ex vivo* porcine tongues, with the average absolute error reducing from $1.73mm$ to $1.46mm$ after applying simulation-driven path adjustments ($p < 0.001$). Additionally, our method not only demonstrated improvements in maintaining the intended cutting shapes and locations, with shape matching scores using Hu moments enhancing from 0.10 to 0.06 and centroid shifts decreasing from $2.09mm$ to $1.33mm$, but it also potentially reduced the likelihood of adverse oncologic outcomes by preventing clinically suggested excessively close margins of $2.2mm$. This feasibility study suggests that merging physics-based cutting simulations with autonomous robotic surgery could potentially lead to more accurate incisions.**

I. INTRODUCTION

Surgical cutting of soft tissues is essential across various treatment modalities, encompassing traditional manual surgery, minimally invasive surgery (MIS), and robot-assisted minimally invasive surgery (RAMIS). Across these approaches, precision in tissue cutting is paramount for both the operation's success and patient safety. Tissues cut in these procedures range from one-dimensional structures akin to vessels, to two-dimensional membranes like fascia or skin, and complex three-dimensional organs, referred to as volumetric entities, in which dimensions are comparably significant [1]. The challenge of volumetric soft tissue cutting is heightened by significant deformation resulting from the interaction between the surgical instrument and the tissue. For example, in tumor resection, it is challenging but crucial to maintain an appropriate margin between the cut and the tumor edge to ensure the complete excision of malignant tissue while minimizing healthy tissue removal. Margins too close to the tumor risk unsafe outcomes and increase the probability of cancer recurrence [2]. Excessive removal of tissue, however, may negatively impact the patient's quality of life [2].

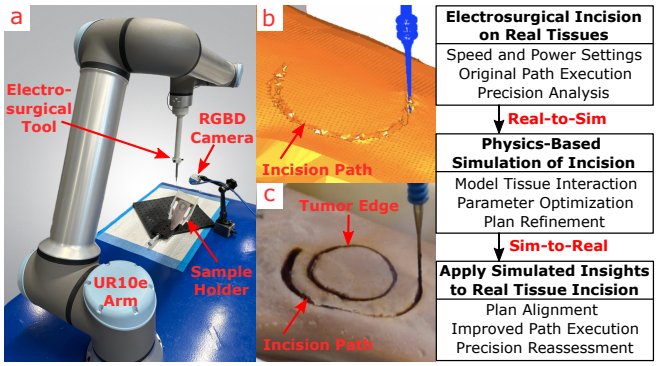

Fig. 1. Images of a) the electrosurgical robotic setup with a sample holder fixating an ex vivo porcine tongue, b) a simulated electrosurgical incision using SOFA, and c) the corresponding incision on a real porcine tongue. The complete real-to-sim-to-real workflow is explained on the right.

Surgeons require rigorous training to master the precision needed for soft tissue cutting using hand-held surgical tools and teleoperated surgical robotic systems. Given the high costs and extensive efforts involved in creating physical phantoms, virtual simulations have been developed to enhance surgeon training. These simulations allow novice surgeons to practice essential techniques in a safe and risk-free environment before entering the operating room [3]. Several virtual simulation platforms are available for training purposes, including Actaeon (BBZ Srl, Verona, Italy), dV Trainer (Mimic Technologies, Seattle, WA), and da Vinci Skills Simulator (Intuitive Surgical, Sunnyvale, CA) [3]. Moreover, virtual surgery simulations are utilized for data collection to train learning-based models [4].

† These authors contributed equally to this work.
* Corresponding author: Jiawei Ge.

This work was supported by the National Institutes of Health through award numbers R01EB020667A1, the National Science Foundation's Foundational Research in Robotics CAREER program under award number 2144348, and the Advanced Research Projects Agency for Health (ARPA-H) under award number AY1AX000023.

[1]Jiawei Ge, Justin D. Opfermann, and Axel Krieger are with the Department of Mechanical Engineering, Johns Hopkins University, Baltimore, MD 21211, USA {jge9; jopferm1; axel}@jhu.edu
[2]Ethan Kilmer is with the Department of Computer Science, Johns Hopkins University, Baltimore, MD 21211, USA ekilmer1@jhu.edu
[3]Leila J. Mady is with the Department of Otolaryngology - Head and Neck Surgery, Johns Hopkins School of Medicine, Johns Hopkins University, Baltimore, MD 21287, USA lmady1@jhu.edu

Simulating soft tissue surgery with realistic physics is a complex engineering challenge that necessitates an accurate material deformation model to ensure successful integration [5]. In practice, the physical properties of *in vivo* tissues must be classified and analyzed, acknowledging that these properties may differ among patients. Deformable objects such as tissues may contain infinite degrees of freedom which can be expensive to compute [5], and a balance must be achieved between the system fidelity and computational efficiency. The simulation of soft tissue cutting further compounds this complexity, as it involves topological changes and dynamic model updates, unlike the primarily surface-oriented deformation seen in grasping scenarios [6]. Moreover, many simulation frameworks import objects as volumetric meshes that are broken down into smaller tetrahedral elements for performance optimization. However, the act of removing tetrahedral elements of disparate sizes to simulate a cutting contradicts the objective of replicating a precise surgical cut.

While the majority of soft tissue modeling research focuses on deformation analysis for surgical simulation, integrating these models into robotic control loops remains largely unexplored. This disconnect represents a significant research gap between surgery simulation and actual surgical practices [7]. Thach et al. introduced DeformerNet, a neural network architecture designed for shape servoing tasks, demonstrating its surgical applicability through the precise manipulation of soft tissues using simulated training data [8]. Similarly, Lin et al. developed a position-based dynamics simulation to train SuPerPM, a software enhancing the surgical scene's perception by accurately identifying and tracking essential tissues and organs [9]. However, these works have yet to extend to surgical cutting, as DeformerNet didn't address cutting tasks, and SuPerPM lacked post-cut tissue tracking capabilities. Chanthasopeephan et al. utilized finite element analysis (FEA)-based simulation to study surgical cutting parameters focusing on straight-line incisions [10], neglecting the complex cutting patterns encountered in procedures like resection surgeries. Scheikl et al. introduced LapGym, leveraging Simulation Open Framework Architecture (SOFA) to develop autonomous laparoscopic skills through reinforcement learning, albeit without real-world experimental validation [11], [12]. Among the rare frameworks available for simulating cuts in deformable objects, DiSECt was noteworthy as a differentiable simulator calibrated to precisely replicate force and deformation in a variety of cutting experiments on soft materials [13]. However, its focus on simulating straight-line cuts with a large, all-purpose knife failed to address the nuanced requirements of complex surgical cutting scenarios.

In this study, we addressed the identified research gap by developing an accurate soft tissue cutting simulation, and integrating it into robotic control loops [7]. This integration allowed for the preoperative prediction and compensation of deformation resulting from tool-tissue interactions, guiding our robotic system towards autonomous planning and execution with improved precision. We conducted and evaluated autonomous incisions on *ex vivo* animal tissues in clinically mimicked scenarios, affirming the efficacy of our methodology. Our contributions include: 1) Developing a novel physics-based simulated surgical scene using SOFA that accurately models tissue deformation during cutting. This model not only considers the mechanical properties of tissues but also the sharpness and speed of the cutting tool as key factors of deformation extent. It assesses errors arising from tool-tissue interactions, and refines cutting plans to better align actual incisions with the intended surgical plan. 2) Demonstrating a statistically significant increase in cutting precision through *ex vivo* experiments utilizing our approach. Additionally, our method has shown improvements in maintaining the intended shapes and locations of cuts, which could potentially decrease the likelihood of adverse oncologic outcomes. This is the first work that attempts to improve clinically relevant soft tissue cutting accuracy using data gathered from a physics-based soft tissue cutting simulation.

II. METHODS

A. Characterization of Electrosurgical Incision Task

Surgical cutting, involving tasks like incision, dissection, and excision, commonly utilizes instruments such as scalpels, scissors, harmonic scalpels, and electrosurgery devices. In particular, our study addresses incisions executed via electrosurgical techniques [14], pivotal in numerous surgical procedures. Surgical incision involves a precise cut breaching the epidermis for diagnostic or therapeutic intervention. Electrosurgery, employing high-frequency electrical currents to cut or coagulate tissue, is a standard technique in pathology management, where precision is key to successful oncologic outcomes. Most research on robotic cutting control of deformable objects focusing on straight or near-straight line cuts using general-purpose knives [10], [13], [15]. In contrast, our study explores more complex and clinically relevant scenarios. Unlike linear incisions, which often result only in cutting depth and length errors, surgical tool-tissue interactions typically cause 3D tissue deformations and deviations from intended cutting paths. Therefore, we investigate incisions along irregular, non-planar contours using a monopolar electrosurgical needle electrode, commonly employed in surgeries like nephrectomy, hepatectomy, cholecystectomy, and glossectomy.

This study focuses on midline partial glossectomy, essential for early-stage tumor resection on the tongue's superior midline surface [16], classified as type 1 glossectomy or mucosectomy [17]. Our approach involves defining the tumor surface shape based on a clinical case report [18], adjusting it to a $2cm$ diameter to match T1/T2 stage cancer dimensions [19]. We also adhere to a $5mm$ resection margin both laterally and in depth, following standard clinical practices [20]. Surgical setup often includes oral gags and traction sutures for anterior tongue access, simulating an open surgical environment [19]. For experiments, we opt for porcine tongue specimens, chosen for their anatomical resemblance to human tongues and ease of accessibility. We 3D print a sample holder mimicking the jawbone and mouth floor, with a clamp to stabilize the posterior tongue. Each tongue sample's tip was sutured and extended by $2cm$ using a linear stage,

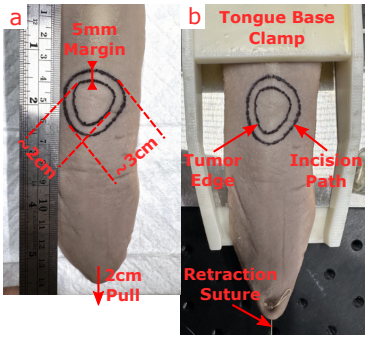

Fig. 2. Sample preparation for electrosurgical incision. a) An *ex vivo* porcine tongue is marked with a $2cm$ diameter contour representing the tumor edge, and a $3cm$ diameter incision path, maintaining a $5mm$ resection margin. b) The tongue is immobilized at the base and extended by $2cm$ at the tip with a retraction suture, replicating the clinical setup for glossectomy procedures.

replicating clinical tongue positioning [19]. The experiment's goal, illustrated in Fig. 2, is to achieve accurate autonomous electrosurgery along the identified incision path.

B. Incision Following Preoperatively Intended Paths

The robotic incision accuracy following preoperatively intended paths on porcine tongues is evaluated, with the findings set to inform subsequent simulation models.

1) Clinically Relevant Tissue Incision Speed: Cutting speed is a critical factor that influences both tissue deformation and the duration of surgery. We enlisted an experienced otolaryngologist to determine a clinically applicable speed for electrosurgical incisions. Utilizing two porcine tongues from a local grocery (H Mart, Lyndhurst, NJ), each tongue was marked with three $10cm$ lines for incision. The surgeon employed an electrosurgical pen (Bovie, Clearwater, FL) to incise at a consistent depth of $5mm$, as per our study's parameters [20]. The duration of each cut was timed by reviewing the recorded video. The cutting speeds recorded were $11.11, 6.66, 7.14, 7.14, 6.25, 5.00 mm/s$ respectively, resulting in an average speed of $7.22 \pm 1.89 mm/s$. Based on these findings, a rounded cutting speed of $7mm/s$ was chosen for subsequent experiments.

2) Robotic Experimental Setup: Leveraging our prior development of the autonomous system for tumor resection (ASTR) [21], this study's testbed comprised five main components (Fig. 1.a): 1) a 6-DOF UR10e manipulator (Universal Robots, Odense, Denmark), 2) a customized laparoscopic electrosurgical instrument, 3) an RGBD camera (D405, Intel, Santa Clara, CA), 4) custom robot operating system (ROS) programs for tissue tracking and incision planning, and 5) a tongue sample holder. A standard monopolar needle electrode with a $25mm$ length and $1mm$ diameter (Bovie, Clearwater, FL), a grounding pad, and an electrosurgical power generator (ASG-300ESU, DRE Veterinary, Louisville, KY) were key components. To manage electrosurgical smoke, we utilized both a portable smoke evacuator (Smoke Shark, Bovie, Clearwater, FL), and an air purifier (GC Multigas, IQAir, Goldach, Switzerland). The sample holder was described in Section II-A, and the software's role in the experimental process will be presented in the following sections.

3) Electrosurgical Cutting Power Setting: Electrosurgical cutting power significantly affects the electrode's *sharpness*, akin to the blade of a scalpel. Adequate power ensures the electrode cuts smoothly, reducing tissue bulging and deformation, which introduce inaccuracies. While higher power increases *sharpness*, it also risks thermal damage and tissue denaturation, negatively impacting post-surgical recovery and organ functionality [22]. To identify the lowest effective power, we utilized four grocery porcine tongues (H Mart), each subjected to incisions at varying powers of 25, 30, 35, and $40 Watts$, corresponding to our experimental setup as described in Section II-A. A custom C++ ROS program enabled the Intel D405 camera to track the incision path through color thresholding, plan electrosurgical incision paths with $5mm$ depth, and guide the robot for execution at $7mm/s$ autonomously. Visual observations revealed that at powers of $35W$ or higher, there was no noticeable tissue bulging, while at $40W$, discoloration suggested tissue denaturation. Consequently, $35W$ was chosen for subsequent experiments.

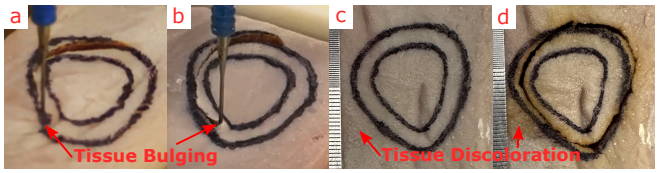

Fig. 3. Visual assessment of tissue responses to various electrosurgical powers: a) noticeable bulging at $25W$, b) reduced but present bulging at $30W$, c) the intact surface prior to incision at $40W$, and d) post-incision discoloration and denaturation at $40W$.

4) Experimental Design to Evaluate Precision: Two *ex vivo* porcine tongues were acquired (Animal Technology, Tyler, TX), and CT-scanned (Loop-X, BrainLab, Munich, Germany). To assess incision accuracy, two samples were prepared as described in Section II-A. The same C++ ROS program was utilized for tracking the marked path, generating the incision plan, and guiding the robotic execution. Key parameters, informed from clinical reports and preliminary findings, included the same near $2cm$ diameter tumor contour, a $5mm$ lateral margin, a $5mm$ incision depth, a $7mm/s$ cutting speed, and a $35W$ electrosurgical power. The detailed evaluation metrics are reported in Section III-A.1.

C. Development and Optimization of Tissue Cut Simulation

This section outlines the development of soft tissue cutting models and simulated surgical setups. It introduces the optimization of simulation parameters to mirror deformation observed in real tissue experiments, and details our approach to refining incision paths for potentially improved precision.

1) Simulation Framework Selection: To accurately replicate tissue cuts, specific criteria were established: 1) replicating clinical setups through the importation of tool and tissue models alongside mechanical and boundary constraints, 2) employing FEA to model nonlinear deformation, and 3) facilitating the division of volumetric objects through cutting interactions. The search for a suitable physics-based simulation framework to meet these criteria led to

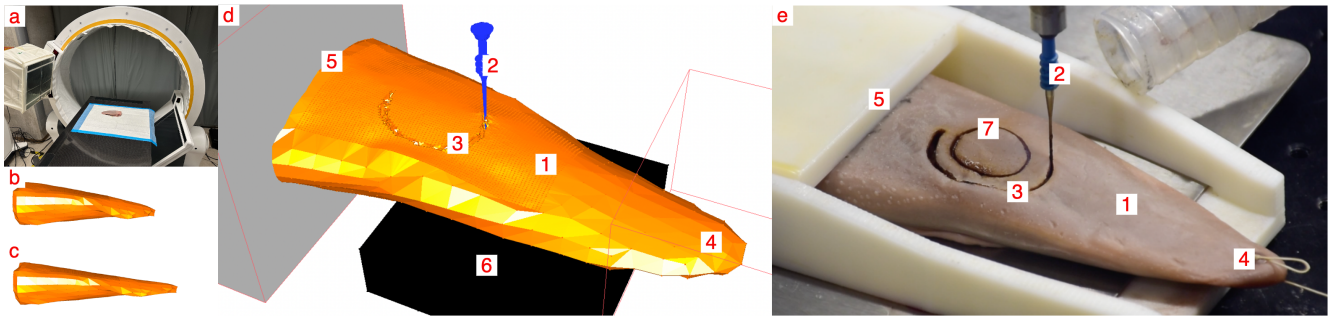

Fig. 4. Side-by-side comparison of physics-based simulated incision and real-world electrosurgical incision. Labels indicate a) CT scanning porcine tongue sample, b) volumetric tongue mesh, c) tongue mesh pulled $2cm$ at the tongue tip, d) and e) side-by-side simulated and experimental surgical scene composed of 1) porcine tongue, 2) electrosurgical instrument, 3) tissue incision contour, 4) $2cm$ anterior tongue stretch and mechanical constraint, 5) posterior tongue mechanical constraint, 6) stabilization support platform, 7) electrocautery tumor edge marking.

the evaluation of FEBio [23], Asynchronous Multi-Body Framework (AMBF) [24], Isaac Gym [25], and SOFA [12]. FEBio focused on deformation and stress analysis, only allowing scripted cuts in predetermined separation locations. AMBF lacked support for volumetric cutting. Isaac Gym was used for data generation in DeformerNet [8], however, despite DiSECt's recent advancements [13], it lacked a dedicated open-source plugin for simulating complex surgical cuts. Other platforms like Gazebo and Ignition were also considered but fell short in soft body mechanics and lacked the necessary cutting features. Ultimately, SOFA was chosen for its extensive use in medical simulation and soft robots, offering comprehensive FEA capabilities and the SofaCarving plugin, enabling realistic volumetric cutting simulations.

2) Soft Tissue Cutting Simulation: SOFA imports tissue models as volumetric meshes consisting of smaller tetrahedral elements. The SofaCarving plugin simulates cutting by removing a tetrahedron of the carving surface mesh upon contact with a carving tool. Rather than incorporating tetrahedron subdivision [26], which is limited to straight-line cuts on tetrahedra for finite element mesh refinement in SOFA, a volumetric mesh densely packed with tetrahedra is preferred to create a refined incision geometry. In these models, the area designated for cutting is densely populated with small tetrahedra, while larger tetrahedra fill the remaining space. This technique improves performance by minimizing unnecessary elements while producing a precise incision edge.

As aforementioned, the surgical instrument *sharpness* plays a critical role in tissue incision accuracy due to material deformation. Given that no real-world tool is perfectly sharp, the SofaCarving's approach of instantaneously removing mesh elements upon contact appears unrealistic. To address this, we introduced a tool *dullness* simulation parameter, defined as the required contact duration between the carving tool and a tetrahedron for its removal. A greater *dullness* leads to more significant tissue deformation and lower incision precision.

3) Simulated Surgical Scene: The experimental surgical scene was recovered in simulation (Fig. 4). A 3D model of the electrocautery tool was supplied to the scene as the cutting tool model. Porcine tongues were CT-scanned using Loop-X, and converted to volumetric meshes following the description in Section II-C.2. Using the SOFA object *TetrahedralCorotationalFEMForceField*, the tissue object was empirically assigned a Young's modulus of $70kPa$ and a Poisson's ratio of 0.49. The electrocautery collision model and tongue collision model acted as the carving tool and carving surface, respectively. To replicate the real-tissue experimental boundary conditions, the tongue model was given a posterior mechanical constraint and underside support platform for stabilization, and the tongue model's tip was pulled $2cm$ from the initial position.

4) Optimizing Simulation Parameters for Real-to-Sim Registration: Assuming that physics-based simulations cannot perfectly replicate real-world phenomena, we further tuned two simulation parameters to align the magnitude of tissue deformation observed in simulations with actual results. To achieve this real-to-sim registration, input simulation tool speed and tool *dullness* were optimized across simulated experiments. Initial robotic incision experiments described in Section II-B.4 were used as a benchmark for real-world outcomes. We varied input tool speed and tool *dullness* on simulated incisions performed on two tissue models representing the two CT-scanned porcine tongues from the real-world experiments in Section II-B.4. The experiments encompassed tool speeds of $1, 5, 9, 13, 17mm/s$, and dullness levels of $1, 5, 9, 13, 17$, culminating in a total of 25 experimental settings. Results and equations used for the real-to-sim parameter registration are reported in Section III-A.2.

5) Improving Preoperatively Intended Tool Paths Using Simulated Data: Following the sim-to-real registration and achieving more accurately simulated tissue deformability, we simulated incisions on newly CT-scanned and uncut porcine samples. Our objective was to predict deformation-induced errors and refine incision plans preoperatively for robotic surgery, thereby completing a real-to-sim-to-real workflow to enhance accuracy. Two new porcine tongues (Animal Technology) were CT scanned using Loop-X, and converted into volumetric meshes for simulation. The tumor shape was imported into the simulation, and an initial tool path was set with a $5mm$ lateral and depth offsets, respectively. Subsequent simulated procedures applied tool speed and *dullness* settings refined through real-to-sim registration, with

incision result evaluation metrics explained in Section III-A.2. Evaluations led to the adjustment of waypoint coordinates on each tool path, shifting them towards or away from the tumor center to correct for specific incision errors identified at those locations. For example, waypoints too close to the tumor were moved away from the tumor center by the measured error distance to counteract deformation-induced inaccuracies, and the opposite was done for waypoints too far. Ideally, the expected incision error post-simulation adjustments would be less than the $0.5mm$ radius of the electrosurgical electrode, beyond which further precision improvements would be impractical. Noteworthy, empirical findings indicated that these adjustments should be applied only once to prevent unpredictable oscillations and potentially decreased accuracy in subsequent robotic executions on actual porcine tongues.

D. Incision Following Simulation-Improved Paths

Real tissue experiments are designed to validate the efficacy of our proposed simulation-improved incision planning approach. It completes the real-to-sim-to-real workflow.

1) Sim-to-Real Registration: The simulation-improved incision path, created in the simulation coordinate frame, required alignment with the real-world coordinate frame to guide our electrosurgical robot, necessitating a sim-to-real registration. After stretching the tongue in the simulation, a point cloud was produced from the volumetric mesh to represent the tongue tissue. Following the complete simulation, this was coupled with the tumor edge and improved incision path. This tongue point cloud was processed to retain the top surface, using a custom Python program with Open3D libraries [27]. In parallel, the same CT-scanned real porcine tongue was prepared in the 3D printed holder, as described in Section II-A. Its superior surface point cloud was cropped and acquired from Intel D405 streamed point cloud using a custom ROS GUI interface. Subsequently, the coherent point drift (CPD) method, augmented with scaling, was applied to achieve registration, employing a Python-based implementation of this algorithm [28]. This process generated a transformation matrix that bridged the simulation and real-world coordinate frames, enabling the precise overlay of the tumor edge and improved incision path from the SOFA simulation onto the actual surgical context.

2) Experimental Design to Evaluate Precision: To assess the effectiveness of robotic incision following simulation-improved versus preoperatively intended incision paths, all key parameters as described in Section II-B.4 were kept consistent. The two newly CT-scanned *ex vivo* porcine tongues (Animal Technology) were prepared as delineated in Section II-A. Since the paths were derived from simulation, the method of manually drawing tumor edges on porcine tongues was impractical. Instead, a C++ ROS program projected the simulated tumor edge and improved incision path onto the tongue sample's surface. The program also implemented a $1mm$ inferior offset to the tumor edge, guiding the electrosurgical robot to mark the edge at $2mm/s$ with minimal tissue deformation. The $5mm$ incision depth was then applied to the projected incision path for autonomous execution. The evaluation metrics are detailed in Section III-A.1.

III. EXPERIMENTAL RESULTS

A. Evaluation Metrics

1) Real Tissue Incision Performances: After completing electrosurgical incisions, top view sample images were captured. The actual incision contours (**aic**) and tumor edge contours (**tec**) are highlighted in red and green colors, respectively (Fig. 5). These images, scaled using a ruler for pixel-to-millimeter conversion, yielded a resolution of about $0.03mm/pixel$.

In this study, we utilized a four-layer metric to evaluate the performance of autonomous incisions for tumor resection surgeries. First, an incision was considered as successful if the red **aic** didn't intersect with and remained exterior to the green **tec**, reflecting a negative margin status where no tumor cells are present at the resected margin. Second, we quantified the dimensional accuracy of the surface margin using a custom Python script employing OpenCV libraries to process the image data and compute surface incision errors (same as used in [21]). The error for each point on the red **aic** was calculated as the shortest distance to the green **tec**, subtracting the intended surface margin of $4.5mm$ (considering a $5mm$ incision margin and a $0.5mm$ electrosurgical electrode radius), and then calculating the absolute values. Mathematically, the error is presented as $\left\| \min_j \|\mathbf{aic}_i - \mathbf{tec}_j\|_2 - 4.5 \right\| mm$ for each point i on the red **aic**. Additionally, the two-tailed t-test will assess differences in these errors before and after applying our simulation-based adjustments, with a significance level of 0.05. Third, shape similarity and centroid displacement between the red **aic** and green **tec** of each porcine sample were evaluated to determine if the desired incision shape and location were achieved. Shape matching scores were calculated using OpenCV libraries based on Hu Moments [29]. Let $D(\mathbf{aic}, \mathbf{tec})$ be the shape difference between red **aic** and green **tec**, and $H_i^{\mathbf{aic}}$ and $H_i^{\mathbf{tec}}$ be the i^{th} log transformed Hu Moments for shapes **aic** and **tec**, respectively. The difference measure was quantified as $D(\mathbf{aic}, \mathbf{tec}) = \sum_{i=0}^{6} \left| \frac{1}{H_i^{\mathbf{tec}}} - \frac{1}{H_i^{\mathbf{aic}}} \right|$, with a value of zero indicating perfect shape match and increasing values denoting greater disparities. Centroid displacements were determined by calculating the Euclidean distance between the centers of mass for the red **aic** and green **tec** of each sample. Fourth, this study further explored oncologic safety by analyzing sites with excessively close margins, which literature suggested may negatively influence local recurrence rates and disease-free survival (DFS) [2]. Similar to the second metric, incision errors were quantified by computing $(\min_j \|\mathbf{aic}_i - \mathbf{tec}_j\|_2 - 4.5)mm$ for each point i on the red **aic**. From an engineering or data analysis viewpoint, incision sites with errors exceeding $-4.5mm$ were considered to have negative margins. However, clinical research indicated a negative margin cutoff of $2.2mm$ as prognostic of diminished DFS [2], [30]. To elaborate, incision sites with errors ranging

from $-4.5mm$ to $-2.3mm$ $(-4.5 + 2.2 = -2.3mm)$ resulted in excessively close margins. Such margins might encapsulate microscopic tumor cells that are challenging to detect, elevating the risk of false negative margin assessments and, consequently, worse DFS.

TABLE I

TABLE OF SIMULATED INCISION RESULTS FOR REAL-TO-SIM PARAMETER REGISTRATION (NOTE: VALUES ROUNDED FOR SPACE.)

Tool		S1	S2	S1&S2		
Vel. (mm /s)	Dull -ness	Absolute Errors (mm)	Absolute Errors (mm)	Absolute Errors (mm)	Max Error (mm)	% Real -to-Sim Reg.
1	1	1.3 ± 0.6	1.2 ± 1.5	1.2 ± 1.0	2.6	80.4%
1	5	1.2 ± 0.6	1.2 ± 1.4	1.2 ± 1.0	2.6	79.6%
1	9	1.2 ± 1.0	1.1 ± 1.7	1.2 ± 1.3	2.8	81.2%
1	13	1.2 ± 0.5	1.1 ± 1.5	1.2 ± 1.0	2.6	78.5%
1	17	1.2 ± 0.5	1.0 ± 1.5	1.1 ± 0.8	2.6	77.0%
5	1	1.0 ± 0.6	1.1 ± 1.5	1.1 ± 1.0	2.6	75.5%
5	5	0.8 ± 0.3	1.0 ± 1.4	0.9 ± 0.9	2.4	66.1%
5	9	0.6 ± 0.8	1.0 ± 0.9	0.8 ± 0.9	1.9	54.9%
5	13	0.6 ± 1.3	0.7 ± 1.7	0.6 ± 1.5	2.4	56.3%
5	17	0.6 ± 0.5	1.1 ± 0.8	0.9 ± 0.7	1.9	58.8%
9	1	1.0 ± 0.4	1.2 ± 1.8	1.1 ± 2.3	3.0	81.5%
9	5	0.4 ± 1.0	0.8 ± 1.4	0.6 ± 1.2	2.2	52.6%
9	9	0.6 ± 0.9	0.7 ± 1.2	0.7 ± 1.0	1.9	49.3%
9	13	0.8 ± 0.7	0.7 ± 1.3	0.8 ± 1.0	2.0	56.2%
9	17	1.0 ± 1.1	1.0 ± 1.2	1.0 ± 1.1	2.2	68.9%
13	1	1.0 ± 0.5	1.0 ± 1.6	1.0 ± 1.0	2.7	74.7%
13	5	0.4 ± 0.7	0.8 ± 1.1	0.6 ± 0.9	1.9	47.2%
13	**9**	$\mathbf{1.7 \pm 1.1}$	$\mathbf{1.4 \pm 1.9}$	$\mathbf{1.6 \pm 1.5}$	**3.3**	**103.6%**
13	13	2.2 ± 1.8	Failure	-	4.0	0.0%
13	17	2.7 ± 2.0	Failure	-	4.6	0.0%
17	1	0.9 ± 0.6	1.0 ± 1.4	1.0 ± 1.0	2.4	67.8%
17	5	0.4 ± 0.9	0.6 ± 1.0	0.8 ± 0.9	1.6	53.9%
17	9	1.1 ± 1.2	Failure	-	2.3	0.0%
17	13	Failure	Failure	-	-	0.0%
17	17	Failure	Failure	-	-	0.0%

2) Simulated Incision Performances: After completing a simulated incision, tongue mesh tetrahedra removed during the procedure were recovered and skeletonized to produce a midline incision contour. This recovered incision contour is evaluated as the **aic** for simulation results reporting.

Simulated incision results were evaluated using a two-layer metric, mirroring real-world result reporting. First, an incision was deemed successful if the maximum error point stayed within $4.5mm$, indicating a negative margin status, and if the simulation produced a closed-loop incision. Second, similar to real-world experiments, the error for each point on the **aic** was calculated as the shortest distance to the **tec** using absolute values, as mathematically described in Section III-A.1.

Simulated incisions results, used for real-to-sim parameter optimization as described in Section II-C.4, were evaluated and registered to real-world results in Section III-B.1, using a three-layer metric. First, the simulation's success was measured by the achievement of a negative margin and the completion of a closed-loop incision. Second, the absolute average incision error across two samples under consistent simulation parameters was examined, and third, the maximum incision error was assessed. Mathematically, real-to-sim registration is defined as $0.75 \cdot \left\| \min_j \|\mathbf{aic}_i - \mathbf{tec}_j\|_2 - 4.5 \right\| + 0.25 \cdot \|\max(\mathbf{aic})\|$ for each point i on the red **aic**, reported as a percentage of the baseline value in Table I. Unsuccessful incisions are reported with a 0% match since all baseline real-world experiments were successful. A real-to-sim parameter registration of 103.6% motivated the selection of simulation parameters: a tool speed of $13mm/s$ and a dullness setting of 9 for subsequent simulations.

B. Results

Quantitative and visual outcomes are detailed in Fig. 5, 6 and Table II, as elaborated in subsequent subsections.

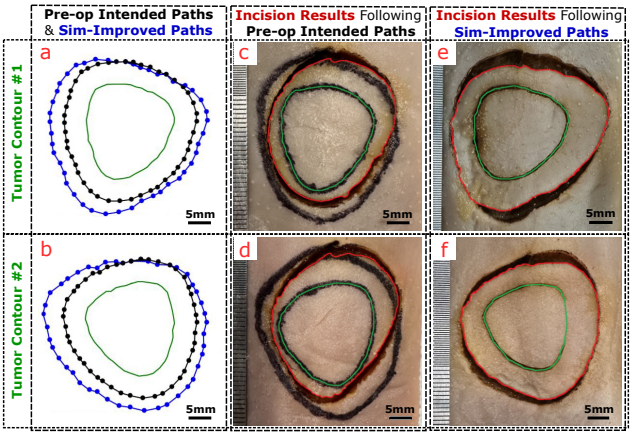

Fig. 5. Visualization of incision paths and outcomes. Plots a) and b) show two tumor shapes in green, corresponding preoperatively intended incision paths in black after applying the 5mm margin to the tumor contour, and simulation improved incision paths in blue. Black and blue dots indicate the incision waypoints for robot execution. Images c) and d) display incision results following preoperatively intended paths in red. Images e) and f) showcase incision results guided by simulation improved paths in red. All incisions follow counterclockwise direction starting from the top of each contour. Each image includes a 5mm scale bar.

1) Incision Results Following Preoperatively Intended Paths: As shown in Fig. 5.c,d, and S1, S2 in Table II. Two out of two *ex vivo* incisions were successful with negative margins. The average absolute incision errors were $1.57 \pm 0.66mm$ and $1.91 \pm 0.90mm$, respectively, leading to a combined average absolute error of $1.73 \pm 0.80mm$. Shape similarity, assessed through Hu Moments, yielded scores of 0.08 and 0.12 for each specimen. Centroid deviations were measured at $1.96mm$ and $2.22mm$, respectively.

2) Simulated Incisions: The simulation-based incision path improvements were conducted on two porcine tongues, which had been CT-scanned and converted into mesh files as described in Section II-C.5. Pre-tool path improvement, two out of two simulated incisions were successful with negative margins and closed-loop incisions. The absolute incision errors were $1.84 \pm 3.53mm$ and $2.14 \pm 4.41mm$, respectively, leading to a combined average absolute error of $1.99 \pm 2.20mm$. Post-tool path improvement, two out of two simulated incisions were successful with negative margins and closed-loop incisions. The absolute incision errors were $0.33 \pm 1.16mm$ and $0.33 \pm 1.02mm$, respectively, leading to a combined average absolute error of $0.33 \pm 0.76mm$.

3) Incision Results Following Simulation-Improved Paths: As shown in Fig. 5.e,f, and S3, S4 in Table II. Two out of two *ex vivo* incisions were successful with negative margins. The

average absolute incision errors were $1.37 \pm 1.19mm$ and $1.57 \pm 0.97mm$, respectively, leading to a combined average absolute error of $1.46 \pm 1.09mm$. Shape similarity, assessed through Hu Moments, yielded scores of 0.06 and 0.06 for each specimen. Centroid displacements were measured at $1.58mm$ and $1.07mm$, respectively.

TABLE II

TABLE OF INCISION RESULTS ON PORCINE SAMPLES

		Success	Absolute Errors(mm)	Shape Similarity	Centroid Shifts(mm)
Pre-op Intended Cuts	S1	✓	1.57 ± 0.66	0.08	1.96
	S2	✓	1.91 ± 0.90	0.12	2.22
	Average	-	$1.73 \pm$ **0.80**	0.10	2.09
Sim-Improved Cuts	S3	✓	1.37 ± 1.19	0.06	1.58
	S4	✓	1.57 ± 0.97	0.06	1.07
	Average	-	**1.46** ± 1.09	**0.06**	**1.33**

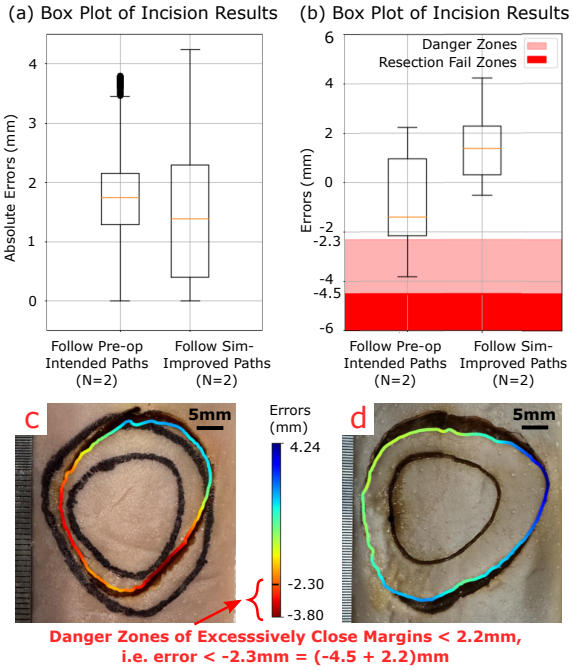

Fig. 6. Box plots of a) absolute errors and b) directional errors for incision results, comparing preoperatively intended and simulation-improved cuts. Red and pink zones indicate failed resections of positive margins, and excessively close margins, respectively. Images c) and d) display two incised samples without and with simulation refinements, with jet color mapping to visualize errors with direction and excessively close margins.

The box plots depicted in Fig. 6.a,b reported both the absolute incision errors and the directional discrepancies of incision errors, and the Fig. 6.c,d displayed error distributions and excessively close margins. Improvements were observed when comparing results post-application of our method to pre-application, including: 1) a statistically significant decrease in average absolute incision errors from $1.73mm$ to $1.46mm$ ($p < 0.001$) based on two-tailed t-test, 2) enhanced fidelity in replicating intended incision geometries with shape matching scores improving from 0.10 to 0.06, 3) more precise incision placements with centroid shifts reducing from $2.09mm$ to $1.33mm$, and 4) prevention of excessively close margins associated with worse DFS, as suggested in [2], [30].

4) Limitations Highlighted by a Case of Reduced Accuracy: A third porcine tongue subjected to the complete real-to-sim-to-real workflow exhibited decreased incision accuracy, marking it as a failed case and revealing a limitation of our proposed method. The sample underwent CT scanning and simulation with optimized parameters aimed at incision path enhancement. Despite these efforts, the simulated absolute incision error marginally improved from $1.93 \pm 3.57mm$ to $0.63 \pm 1.97mm$, failing to meet our anticipated $0.5mm$ accuracy threshold detailed in Section II-C.5. Subsequent simulation iterations adjusted incision waypoints closer or further from the tumor, using the same explained method, attaining an improved accuracy of $0.33 \pm 0.85mm$. However, when this simulation-modified path was executed robotically on the actual porcine tongue, the absolute incision errors worsened to $2.11 \pm 1.64mm$, with a shape matching score of 0.10, and a centroid displacement of $1.62mm$. These outcomes not only showed reduced incision precision but also poorer maintenance of incision shape and location, thereby underscoring a critical limitation of our approach as highlighted in Section II-C.5.

IV. DISCUSSION

In previous research, we achieved sub-millimeter precision in incision accuracy at a slow cutting speed of $2mm/s$, which resulted in extended surgery duration and increased thermal tissue damage [21]. Building upon this, our current study explores a clinically more relevant speed of $7mm/s$, at the cost of increased incision error. Despite simulation-based improvements, we could not replicate the precision of slower speeds at this higher rate. This finding necessitates a discussion among surgical professionals to find an optimal balance between efficiency and accuracy, tailored to specific clinical needs and priorities.

The challenge of accurately simulating soft tissue deformation for robotic surgery remains significant [7], as evidenced by research primarily concentrating on simpler linear cuts from 2007 to 2023 [10], [13]. The variability in patient-specific tissue properties further complicates the development of a universal physics-based model for precise organ deformability prediction. Our study, despite its limited sample size, serves as a preliminary investigation rather than comprehensive research aimed at definitive precision enhancement. It underscores the importance of advancing towards more realistic surgical simulations and developing models that account for individual tissue differences.

Our current approach does not support real-time adjustments to address discrepancies between preoperative and intraoperative imaging, such as those caused by unexpected tissue retraction. To balance computational efficiency with system fidelity, our simulations employ models containing around one hundred thousand tetrahedra, processed using the SofaCarving plugin. This complexity results in processing times of approximately 1-2 hours on a 2020 MacBook Pro.

The failed case study underscores another limitation of our method: its effectiveness largely hinges on the initial simulation's accuracy. Our empirical findings suggest that even

if desired precision in simulated incisions is achieved after several iterations, the robotic execution on porcine tongues may result in diminished precision. This illustrates that our method is selective in terms of patient eligibility, which, although a limitation, does not invalidate the applicability of our method to surgical procedures. Such selectivity exists in many existing surgical techniques like LASIK eye surgeries, where individuals with thin corneas may not be suitable candidates.

V. CONCLUSIONS

In conclusion, this study demonstrates a successful integration of physics-based tissue cutting simulations with autonomous robotic execution, targeting the precision of incisions along complex contours in animal tissues. We introduced an innovative simulation model on the SOFA platform, featuring a concept of simulated cutter *dullness* to mirror the deformability observed in real tissue experiments accurately. This model was utilized to foresee and compensate for the deformations arising from tool-tissue interactions preoperatively, leading to enhanced surgical path planning. The findings confirm our approach enhances incision accuracy, reducing the average absolute error from $1.73mm$ to $1.46mm$ ($p < 0.001$) and improves the preservation of intended cutting shapes and locations—shape matching scores improved from 0.10 to 0.06, and centroid shifts decreased from $2.09mm$ to $1.33mm$. This precision in execution potentially improves DFS by reducing risks associated with margins closer than the clinically suggested threshold of $2.2mm$ [30].

Looking ahead, our research will explore more sophisticated simulations of deep tumor margins, extending beyond mere incision to encompass entire tumor resection processes. We also aim to enhance simulation fidelity by estimating and utilizing the patient-specific Young's modulus and Poisson's ratio of tumors and surrounding tissues through ultrasound elastography [31]. Furthermore, we will explore innovative solutions to broaden the applicability of our method to a wider patient demographic, reducing the current limitations regarding patient selection.

REFERENCES

[1] J. Sanchez, J.-A. Corrales, B.-C. Bouzgarrou, and Y. Mezouar, "Robotic manipulation and sensing of deformable objects in domestic and industrial applications: a survey," *The International Journal of Robotics Research*, vol. 37, no. 7, pp. 688–716, 2018.

[2] M. M. Li, S. V. Puram, D. A. Silverman, M. O. Old, J. W. Rocco, and S. Y. Kang, "Margin analysis in head and neck cancer: state of the art and future directions," *Annals of surgical oncology*, vol. 26, pp. 4070–4080, 2019.

[3] D. Zerbato and D. Dall'Alba, "Role of virtual simulation in surgeon training," *Journal of Visualized Surgery*, vol. 3, 2017.

[4] G. Ntakakis, C. Plomariti, C. Frantzidis, P. E. Antoniou, P. D. Bamidis, and G. Tsoulfas, "Exploring the use of virtual reality in surgical education," *World Journal of Transplantation*, vol. 13, no. 2, p. 36, 2023.

[5] T.-N. Nguyen, M.-C. Ho Ba Tho, and T.-T. Dao, "A systematic review of real-time medical simulations with soft-tissue deformation: Computational approaches, interaction devices, system architectures, and clinical validations," *Appl Bionics Biomech*, 2020.

[6] J. Wu, R. Westermann, and C. Dick, "A survey of physically based simulation of cuts in deformable bodies," in *Computer Graphics Forum*, vol. 34, no. 6. Wiley Online Library, 2015, pp. 161–187.

[7] J. Zhang, Y. Zhong, and C. Gu, "Deformable models for surgical simulation: a survey," *IEEE reviews in biomedical engineering*, vol. 11, pp. 143–164, 2017.

[8] B. Thach, B. Y. Cho, S.-H. Ho, T. Hermans, and A. Kuntz, "Deformernet: Learning bimanual manipulation of 3d deformable objects," *IEEE Transactions on Robotics*, 2023.

[9] S. Lin *et al.*, "Superpm: A large deformation-robust surgical perception framework based on deep point matching learned from physical constrained simulation data," *ICRA 2024*, 2023.

[10] T. Chanthasopeephan, J. P. Desai, and A. C. Lau, "Modeling soft-tissue deformation prior to cutting for surgical simulation: finite element analysis and study of cutting parameters," *IEEE transactions on biomedical engineering*, vol. 54, no. 3, pp. 349–359, 2007.

[11] P. M. Scheikl *et al.*, "Lapgym–an open source framework for reinforcement learning in robot-assisted laparoscopic surgery," *arXiv preprint arXiv:2302.09606*, 2023.

[12] F. Faure *et al.*, "Sofa: A multi-model framework for interactive physical simulation," *Soft tissue biomechanical modeling for computer assisted surgery*, pp. 283–321, 2012.

[13] E. Heiden, M. Macklin, Y. Narang, D. Fox, A. Garg, and F. Ramos, "Disect: a differentiable simulator for parameter inference and control in robotic cutting," *Auton Robot*, vol. 47, pp. 549–578, 2023.

[14] A. Taheri, P. Mansoori, L. F. Sandoval, S. R. Feldman, D. Pearce, and P. M. Williford, "Electrosurgery: part i. basics and principles," *Journal of the American Academy of Dermatology*, vol. 70, no. 4, pp. 591–e1, 2014.

[15] L. Han, H. Wang, Z. Liu, W. Chen, and X. Zhang, "Vision-based cutting control of deformable objects with surface tracking," *IEEE/ASME Transactions on Mechatronics*, vol. 26, no. 4, pp. 2016–2026, 2020.

[16] T. Toh, T. Akita, M. Saito, and T. Shigetomi, "Squamous cell carcinoma initially arising in the midline of the dorsum of the tongue in a young adult: a case report and review of the literature," *Journal of Oral and Maxillofacial Surgery, Medicine, and Pathology*, vol. 31, no. 3, pp. 185–188, 2019.

[17] M. Ansarin *et al.*, "Classification of glossectomies: Proposal for tongue cancer resections," *Head & neck*, vol. 41, no. 3, pp. 821–827, 2019.

[18] T. Suga *et al.*, "Case report: Hidden oral squamous cell carcinoma in oral somatic symptom disorder," *Frontiers in Psychiatry*, vol. 12, p. 651871, 2021.

[19] J.-L. M. Bigcas and O. T. Okuyemi, "Glossectomy," in *StatPearls [Internet]*. Treasure Island (FL): StatPearls Publishing, 2023, updated 2023 Jul 25. Available from: https://www.ncbi.nlm.nih.gov/books/NBK560636/.

[20] M. Alicandri-Ciufelli *et al.*, "Surgical margins in head and neck squamous cell carcinoma: what is 'close'?" *European Archives of Oto-Rhino-Laryngology*, vol. 270, pp. 2603–2609, 2013.

[21] J. Ge *et al.*, "Autonomous system for tumor resection (astr) - dual-arm robotic midline partial glossectomy," *IEEE Robotics and Automation Letters*, vol. 9, no. 2, pp. 1166–1173, 2024.

[22] T. V. Nechay *et al.*, "Thermal effects of monopolar electrosurgery detected by real-time infrared thermography: an experimental appendectomy study," *BMC surgery*, vol. 20, no. 1, pp. 1–12, 2020.

[23] S. A. Maas, B. J. Ellis, G. A. Ateshian, and J. A. Weiss, "Febio: finite elements for biomechanics," 2012.

[24] V. M. Varier, D. K. Rajamani, F. Tavakkolmoghaddam, A. Munawar, and G. S. Fischer, "Ambf-rl: A real-time simulation based reinforcement learning toolkit for medical robotics," in *2022 International Symposium on Medical Robotics (ISMR)*. IEEE, 2022, pp. 1–8.

[25] V. Makoviychuk *et al.*, "Isaac gym: High performance gpu-based physics simulation for robot learning," 2021.

[26] L. Rodríguez, I. Navazo, and A. Vinacua, "Data-driven tetrahedral mesh subdivision," in *Computer Graphics forum*, vol. 26, no. 4. Wiley Online Library, 2007, pp. 783–793.

[27] Q.-Y. Zhou, J. Park, and V. Koltun, "Open3D: A modern library for 3D data processing," *arXiv:1801.09847*, 2018.

[28] Kenta-Tanaka et al., "probreg." [Online]. Available: https://probreg.readthedocs.io/en/latest/

[29] M.-K. Hu, "Visual pattern recognition by moment invariants," *IRE transactions on information theory*, vol. 8, no. 2, pp. 179–187, 1962.

[30] D. K. Zanoni *et al.*, "A proposal to redefine close surgical margins in squamous cell carcinoma of the oral tongue," *JAMA Otolaryngology–Head & Neck Surgery*, vol. 143, no. 6, pp. 555–560, 2017.

[31] M. T. Islam, S. Tang, C. Liverani, S. Saha, E. Tasciotti, and R. Righetti, "Non-invasive imaging of young's modulus and poisson's ratio in cancers in vivo," *Scientific reports*, vol. 10, no. 1, p. 7266, 2020.